

Spin-leap performance by cetaceans is influenced by moment of inertia

Frank E. Fish^{1,*}, Anthony J. Nicastrò², Kaitlyn L. Cardenas¹, Paolo S. Segre³, William T. Gough³, Shirel R. Kahane-Rapport³, Judy St. Leger⁴, Jeremy A. Goldbogen³

¹Department of Biology, West Chester University, West Chester, PA 19383 USA

²Department of Physics and Engineering, West Chester University, West Chester, PA 19383 USA

³Hopkins Marine Station of Stanford University, Pacific Grove, CA 93950 USA

⁴Sea World, San Diego, CA 92109 USA

* Author for correspondence (ffish@wcupa.edu), Address: Department of Biology, West Chester University, West Chester, PA 19383, USA. Phone: 610-436-2460

Keywords: angular momentum, breaching, swimming, spinning, roll, flippers

Summary Statement

The rate of spinning about the longitudinal axis of various cetaceans performing dramatic aerial leaps from the water varies with respect to their morphology that affects the moment of inertia.

Abstract

Cetaceans are capable of extraordinary locomotor behaviors both in water and air. Whales and dolphins can execute aerial leaps by swimming rapidly to the water surface to achieve an escape velocity. Previous research on spinner dolphins demonstrated the capability of leaping and completing multiple spins around their longitudinal axis with high angular velocities. This prior research suggested the slender body morphology of spinner dolphins together with the shapes and positions of their appendages, allowed for rapid spins in the air. To test if greater moments of inertia reduced spinning performance, videos and biologging data of cetaceans above and below the water surface were obtained. The principal factors affecting the number of

aerial spins a cetacean can execute were moment of inertia and use of control surfaces for subsurface corkscrewing. For spinner dolphin, Pacific striped dolphin, bottlenose dolphin, minke whale, and humpback whale, each with swim speeds of 6-7 m s⁻¹, our model predicted that the number of aerial spins executable were 7, 2, 2, 0.76, and 1, respectively, which were consistent with observations. These data implied that the rate of subsurface corkscrewing was limited to 14.0, 6.8, 6.2, 2.2, and 0.75 rad s⁻¹ for spinner dolphins, striped dolphins, bottlenose dolphins, minke whales, and humpback whales, respectively. In our study, the moment of inertia of the cetaceans spanned a 21,000-fold range. The greater moments of inertia for the latter four species produced large torques on control surfaces that limited subsurface corkscrewing motion and aerial maneuvers compared to spinner dolphins.

Introduction

The proficiency of aquatic animals with respect to maneuverability is constrained by their morphology with regard to the flexibility of the body and the hydrodynamic characteristics and position of the control surfaces (e.g., fins, flippers, flukes, keels) influencing the animal's performance (Harris, 1936, 1937; Webb, 1984, 2004, 2006; Fish, 2002; Fish et al., 2003; Miklosovic et al., 2004; Weber et al., 2014; Fish and Lauder, 2017; Leahy et al., 2021; Segre et al., 2022). The morphology directly influences the control of the three rotational degrees of freedom of yaw, pitch, and roll. Whereas turning using yaw and pitch has been the focus of much of the research on maneuverability in aquatic animals (e.g., Harris, 1936; Howland, 1974; Webb, 1983; Domenici and Blake, 1997; Fish and Nicastrò, 2003; Weber et al., 2014; Segre, 2022; Downs et al., 2023), roll has received considerably less attention. This bias is due mainly to studies on organisms with gravity-centric orientations, hydrostatic stability, vertically oriented rudder-like median fins, and operation on a planar water surface. However, rolling around the longitudinal axis is important for turning by organisms that use laterally projecting control surfaces, have a center of gravity located near the center of buoyancy, and operate submerged in a three-dimensional environment (Fish, 2002; Goldbogen et al., 2013; Fish and Holzman, 2019; Segre et al., 2022). Particularly, marine mammals (cetaceans, pinnipeds, sirenians) will roll the body to turn by banking in order to facilitate use of their lateral control surfaces to hydrodynamically generate a centripetal force (Fish and Battle, 1995; Fish, 2002; Fish et al.,

2003; Cheneval et al., 2007; Wiley et al., 2011; Segre et al., 2018, 2022). Underwater rolling is used by dolphins to increase the echolocatory insonification to the receiving areas to compensate for the asymmetrical and narrow echolocation beam (Wei et al., 2023). Rolling can also be used by the animal to change its energy state and linearly decelerate by transferring linear kinetic energy for translational speed to rotational kinetic energy as in the case of banked aerial turns (Giancoli, 1991; Lissaman, 2007).

Spinning can be considered a rolling maneuver in which rotations in the longitudinal axis of the body are produced. Such spinning behaviors are used for dismemberment of large food items (Helfman and Clark, 1986; Fish et al., 2007) and targeting prey underwater (Goldbogen et al., 2013). The most exaggerated of the spinning behaviors is displayed by the spinner shark, *Carcharhinus brevipinna*, and other carcharhinid sharks, especially the black-tipped shark, *Carcharhinus limbatus*, and by spinner dolphins, *Stenella longirostris*, and Clymene or short-snouted spinner dolphins, *Stenella clymene*. These species perform spectacular aerial leaps while spinning up to seven times after clearing the water (Hester et al., 1963; Norris and Dohl, 1980; Perrin and Gilpatrick, 1994; Fish et al., 2006; Schwartz, 2013). The spinning behavior was inferred to be associated with the removal of remoras (Norris et al., 1994; Ritter, 2002; Ritter and Brunschweiler, 2003; Fish et al., 2006; Weihs et al., 2007; Schwartz, 2013).

The mechanics of the spinning leap by the spinner dolphins were modeled in Fish et al. (2006). The mathematical model demonstrated that angular momentum was generated while the dolphin was underwater. The resistive and driving torques generated by the dolphin's control surfaces were balanced to induce a low spin rate. Upon breaching the surface of the water, the torques became unbalanced with the driving torque dominating to produce an accelerated rate of spin. Analysis of the spinning leaps also indicated the body slenderness of the spinner dolphin with a fineness ratio of 6.3 enhanced spinning performance (Fish et al., 2006). A slender body would reduce the moment of inertia and foster greater angular acceleration than a thick body (Giancoli, 1991; Fish et al., 2006).

The present study was undertaken to investigate the relationship of the moment of inertia and the rate of spinning with respect to variation in size for cetaceans (i.e., dolphins and whales). We hypothesized that increasing body mass and girth in cetaceans would limit the number of aerial spins when leaping due to an increase in the moment of inertia. Cetaceans range in body length from 1.2 m to 31.0 m (Nowak, 1999), but maintain a similar body design with a

streamlined, fusiform shape. In the water, the body shape of cetaceans permits rolling maneuvers (Fish, 2002; Goldbogen et al., 2013; Segre et al., 2016). Many dolphins and whales leap or breach from the water into the air and are capable of varying degrees of aerial spinning (Au and Weihs, 1980; Whitehead, 1985; Au et al., 1988; Würsig et al., 1989; Weihs, 2002; Fish et al., 2006; Pearson, 2017; Halsey and Iosilevskii, 2020; Segre et al., 2020). A test of the hypothesis utilized data from video recordings of trained and wild dolphins, and biologging data from large whales executing aerial spins.

Materials and methods

Model for aerial spinning

The aerial capabilities of cetaceans are dynamically linked to their subsurface motions. The model of Fish et al. (2006), which was restricted to two species of spinner dolphins, assumes that animals establish a subsurface rotational equilibrium, balancing a propulsive rotational torque with drag torques acting on the control surfaces. As an animal emerges into air, those drag torques vanish as each control surface leaves the water, permitting the animal to angularly accelerate and thus increase its rate of rotation compared to its subsurface rate. For *Stenella longirostris*, a maximal 7 aerial spins in one second can result from a subsurface corkscrewing rate of 2 rev s⁻¹. Screwing is a underwater rolling maneuver in which the animal turns about its longitudinal axis (Fish et al., 2006). The model from Fish et al. (2006) also utilizes a rotational performance coefficient, defined to be $\theta_R = \omega_A/v_s$, the ratio of the subsurface angular speed, ω_A (rad s⁻¹) to the swim speed, v_s (m/s). θ_R (rad m⁻¹) represents a parameter that expresses the intuitive notion that the angular speed achievable while corkscrewing is directly proportional to the swim speed. θ_R is controlled by the animal and can vary from zero, when the animal swims in a straight line with no rotation about its longitudinal axis, to some maximum value permitted by the animal's morphology and regulated by the flexions of the control surfaces and, to a more limited extent, the torsion limit of the tailstock.

In this study, we retained the fundamentals of the model developed in Fish et al. (2006) for spinner dolphins (*Stenella longirostris* Gray, 1828), but (1) extend it to additional species of cetaceans, including other members of the Delphinidae with Pacific white-sided dolphin (*Lagenorhynchus obliquidens* Gill 1865) and bottlenose dolphin (*Tursiops truncatus* Montagu

1821), and members of the Balaenopteridae with the minke whale (*Balaenoptera acutorostrata* Lacépède, 1804), and humpback whale (*Megaptera novaeangliae* Borowski 1781) (Fig. 1), (2) investigate the effect of control surface area on the number of executable aerial spins, (3) determine the rotational performance and spin index for each of the species studied, and (4) generalize the model to any animal with differing surface areas and numbers and locations of control surfaces.

The model developed by Fish et al. (2006) showed that for spinner dolphins with pectoral flippers, a dorsal fin and caudal flukes as control surfaces, the number, N , of complete aerial spins executed by an animal with total moment of inertia, I , swimming underwater at a speed, v_s , and corkscrewing with an angular speed, ω_A , is:

$$\frac{\pi N g}{v_s} = \omega_A + \frac{\tau_{net,B} \Delta x_B}{v_s I} + \frac{\tau_{net,C} \Delta x_C}{v_s I}, \quad (\text{Eq. 1})$$

where Δx_B is the distance between the pectoral flippers and the dorsal fin and Δx_C is the distance between the dorsal fin and the flukes. The moment of inertia (I) of a point-like body is the mass (M) times the square of the perpendicular distance to the rotation axis (Giancoli, 1991). For the bodies of the cetaceans, the moment of inertia was modeled as a three-dimensional prolate spheroid. The moment of inertia was calculated as $I = 2 M R^2/5$ (Fig. 2), where M is the body mass plus the added mass in kg and R is the maximum radius of the body in m without the control surfaces. The added mass is the extra mass of fluid entrained to the body while in motion (Webb, 1975). For a whale-like body, the added mass is the body mass times the added mass coefficient (k_1). According to Lamb (1932) for an ideal fluid, k_1 is 0.059 and 0.045 for prolate ellipsoids with length to diameter ratios of 4.99 and 6.01, respectively. $\tau_{net,B}$ and $\tau_{net,C}$ are the net torques acting on the animal between the time the pectoral flippers begin to emerge from the water and the dorsal fin begins to emerge (Stage B) and the net torque acting between the time the dorsal fin begins to emerge and the flukes begin to emerge (Stage C), respectively (Fish et al., 2006). We can generalize Eq. 1 so that it permits us to adapt the model to cetaceans with nearly absent dorsal fin, such as with *Megaptera*:

$$\frac{\pi N g}{v_s} = \omega_A + \frac{1}{v_{sI}} \sum_i \tau_{net,i} \Delta x_i. \quad (\text{Eq. 2})$$

In general, Eq. 2 is useful in the analysis of the aerial maneuvers of animals with a more complicated array of control surfaces.

In our model, the resistive drag torques act on control surfaces as an animal initiates a subsurface corkscrewing maneuver. In this context, it is important to note that aerial spins are executable only if the animal's morphology permits large enough drag torques to be established. As drag torques are shed in a leap, a net torque results that produces an angular acceleration. The torques necessary to balance drag torques as the animal corkscrews, in turn, depend jointly upon the animal's morphology and physiology. Assuming that an animal's dorsal fin produces no torques other than a drag torque, corkscrewing at a constant angular speed ω_A involves balancing the hydrodynamic drive torque at the canted pectoral flippers and the drive torque produced at the flukes. This follows from the lack of a systematic torsion in the body while corkscrewing.

As shown in Fish et al. (2006) the resistive torques can be expressed as a function of ω_A , the subsurface angular speed. For the pectoral flippers specifically, the torques produced by the pectoral fins, τ_p , $\tau_p = R_p \omega_A^2$, where R_p is a constant computed from the area of the pectoral flippers, their orientation relative to the longitudinal spin axis, and other constants described in Fish et al. (2006). Similarly for the other control surfaces, the torque produced by the dorsal fin is $\tau_D = R_D \omega_A^2$, and for the flukes, $\tau_F = R_F \omega_A^2$. In addition to the resistive torque on the flukes produced by rotation about the animal's longitudinal axis, the oscillatory motion of the tail and flukes is responsible for producing the torque necessary to drive the animal forward. Because the lack of a systematic torsion in a corkscrewing cetacean implies that the total drive torque, τ_{drive} , must be split equally between the hydrodynamic torques generated at the pectoral flippers and the drive torque produced by the flukes, we have the condition that:

$$\tau_{drive} = \tau_p = \frac{1}{2} \tau_{total}. \quad (\text{Eq. 3})$$

For an aerial spin to commence, $\tau_p - \frac{1}{2} \tau_{total} \geq 0$, that is,

$$R_p \omega_A^2 - \frac{1}{2} (R_p + R_D + R_F) \omega_A^2 \geq 0. \quad (\text{Eq. 4})$$

So,

$$\frac{1}{2} R_P - \frac{1}{2} (R_D + R_F) \geq 0, \quad (\text{Eq. 5})$$

and finally

$$R_P \geq R_D + R_F. \quad (\text{Eq. 6})$$

Eq. 6 represents the condition on a cetacean's morphology to be able to execute aerial spins.

As shown in Fish et al. (2006), the differential amount of resistive torque ($d\tau$) produced by an element of area on a control surface, dA , a distance R away from the rotational axis is:

$$d\tau = R dF = R \left(\frac{1}{2} \rho C \omega_A^2 R^2 \right) = \frac{1}{2} \rho C \omega_A^2 R^3 dA, \quad (\text{Eq. 7})$$

Where the density of sea water $\rho = 1025 \text{ kg m}^{-3}$ and the drag coefficient $C = 1.2$ (Potter and Foss, 1975). For a constant corkscrewing rate ω_A :

$$\tau = \frac{1}{2} \rho C \omega_A^2 \int R^3 dA, \quad (\text{Eq. 8})$$

where the integration is over the area of the control surface. Thus, the condition for executing aerial spins in Eq. 6 can be rewritten to be:

$$\frac{1}{2} \rho C \omega_A^2 \int_{\text{pectoral flippers}} R^3 dA \geq \frac{1}{2} \rho C \omega_A^2 \int_{\text{dorsal fin}} R^3 dA + \frac{1}{2} \rho C \omega_A^2 \int_{\text{flukes}} R^3 dA, \quad (\text{Eq. 8})$$

or

$$\int_{\text{pectoral flippers}} R^3 dA \geq \int_{\text{dorsal fin}} R^3 dA + \int_{\text{flukes}} R^3 dA. \quad (\text{Eq. 9})$$

Thus, in the model's assumptions of a constant subsurface corkscrewing rate and rigid control surfaces, a cetacean's ability to execute aerial spins is determined solely by the geometrical form and positions of the control surfaces relative to the animal's longitudinal axis. As can be seen in either Eq. 6 or Eq. 9, the placement of the pectoral flippers sets the scale for the ability to spin: the torques produced by the pectoral flippers must exceed the sum of all other resistive torques. We note here that the number (N) of spins executable by a cetacean depends, as can be seen in Eq. 1, on the distribution of mass around the spin axis affecting moment of inertia besides the shape and placement of control surfaces.

Spinning leaps of dolphins and whales

The spinning leaps of trained dolphins were performed at Sea World (SW; San Antonio, TX; S1) and the National Aquarium (NA; Baltimore, MD; S2). Two adult female *Lagenorhynchus* (SW) and two adult male and five female *Tursiops* (NA) were utilized to perform the behavior. Dolphins executed the spinning leaps in the center of large exhibit pools at each facility (S1, S2). Each pool was constructed with large underwater viewing windows. Two video cameras (Canon EOS 5D Mark III equipped with a Canon Zoom Lens EF 24-70 mm, 1:2.8) were mounted on tripods and positioned to record the movements of the dolphins simultaneously below and above the water surface. The dolphins had been trained to perform the spinning leap on command. Leap height was measured as the vertical displacement of the center of gravity (CG) above the water surface. CG was assumed to be at a position of $0.4L$ (Fish, 2002). Morphometrics of the dolphins were supplied by the staff at each facility, which included total body length (L), maximum body diameter (D), flipper width and span, fluke width and span in meters, and body mass in kg. The fineness ratio was calculated as the ratio of L/D . The research on the trained dolphins was approved by the West Chester University Institutional Animal Care and Use Committee (Protocol #201201).

Data on the morphometrics and spinning leap performance for *Stenella* were obtained from Fish et al. (2006) for 858 *Stenella longirostris* that were collected as by-catch from the tuna purse-seine fishery in the eastern Pacific Ocean (S. Chivers, unpub. data). Morphometric data for one individual of *Balaenoptera* and eight individuals of *Megaptera* for L and D were determined from calibrated images using aerial drone photography according to the method of Gough et al. (2019). The maximum radius of the body (R) was one half D . The mass (kg) of *Balaenoptera*

acutorostrata was computed according to Kahane-Rapport and Goldbogen (2018) with the equation $\log_{10}(M)=3.091(\log_{10}(L))+1.009$. The mass (kg) of *Megaptera* was calculated according to the equation $M=1000(0.0158L^{2.95})$ from Lockyer (1976).

Spinning leap data for *Balaenoptera* and *Megaptera* were measured from suction-cup attached biollogger recording tags (Gough et al., 2019; Segre et al., 2020). The tags were equipped with accelerometers, magnetometers, gyroscopes, depth sensors, hydrophones, and on-board video camera (Fig. 3; see Segre et al., 2020 for specifications and deployment). The tags were placed on the dorsum of the animals and held by suction cups, which released for retrieval after a period of time. Breaches were only included for analysis where the suction-cups did not slip or detach throughout the ascent, and where the orientation of the tag could be confidently estimated (S3). The velocity of the whale in water was determined by the method described in Segre et al. (2020). The rotational velocities of the whales were measured with gyroscopes. Additional observations on spinning by *Megaptera* were obtained from YouTube videos (S4).

All research on the tagging and observations of baleen whales were conducted under approval of the National Marine Fisheries Service (permits 16111, 19116, 15271, 14809, 14682, 18059); National Marine Sanctuaries (MULTI-2017-007); Marine Mammal Protection Act (775-1875); Department of Environmental Affairs (RES2018/63); Nelson Mandela University animal ethics approval (A18-SCI-ICMR_001); Regional Directorate for Sea Affairs, Autonomous Region of the Azores (49/2010/DRA), and the Stanford IACUC.

Results

The average body dimensions and moment of inertia (I) are provided in Table 1. There was an overall size difference of about 6.8-fold between *Stenella* and *Megaptera* in regard to both the body length and maximum radius. However, the difference in fineness ratio for the species examined was no greater than 25%. M showed a 443-fold difference for the species examined and I showed a 20,990-fold difference over the size range (Fig. 4).

The number of aerial spin leaps examined were 5 for *Balaenoptera*, 32 for *Lagenorhynchus*, 15 for *Megaptera*, and 38 for *Tursiops*. The maximum rate of aerial spin leaps (ω_{SL}) varied inversely with body size (Table 1; Fig. 5). Range of ω_{SL} varied from 156 deg s⁻¹ to 2081 deg s⁻¹, which represented a 30-fold decrease with increasing M . The highest maximum ω_{SL}

was produced by *Stenella* with the lowest I ; whereas, the lowest ω_{SL} was produced by *Balaenoptera* (Fig. 6). Despite the larger M and I of *Megaptera* compared to *Balaenoptera*, ω_{SL} for *Megaptera* was 2.6 times greater.

The summarized results of the model for the hydrodynamics torques are shown in Fig. 7. The number of complete spins is dependent on the relationship between the swim speed and angular speed while underwater. High numbers of aerial spins by dolphins are achieved with higher angular and swimming speeds compared to low spin numbers as seen for the whales. With increasing swim speeds and lower I , more spins are possible for a given angular speed.

As indicated previously, θ_R , the rotational performance coefficient, is controlled by the animal, but its maximum value is determined by the animal's morphology. The value of θ_R can be estimated via our model for spin-leap performance. That inference requires measurements of an animal's maximum swim speed and observations of the maximum number of spins executed by an animal. With these measurements, θ_R can be estimated.

To illustrate the application of the model in determining the rotational performance coefficient, θ_R , consider the case of *Tursiops*, whose maximum swim speed is 7.1 m s^{-1} and has been observed to execute up to 2 full aerial spins. The graph for *Tursiops* in Fig. 7 shows the computed relations between subsurface corkscrewing angular speed, ω_A , and the animal's swim speed, v_s , for various numbers of aerial spins. For $N = 2$ spins and a maximum swim speed of 7.1 m s^{-1} , a star (*) appears on the graph at that position. The corresponding value of ω_A is 6.2 rad s^{-1} , according to the graph. Thus, $\theta_R = \omega_A/v_s = (6.2 \text{ rad s}^{-1})/(7.1 \text{ m s}^{-1}) = 0.87 \text{ rad m}^{-1}$, and that value is listed in Table 2. Note, though, that the values of ω_A listed in Table 2 are computed directly from the model using Eq. 1 and morphometric data, and not read from a graph.

The results for the five species studied appear in Table 2. Note that, apart from *Stenella longirostris*, the maximum swim speeds of the four other species in our study do not vary by more than 3% from the average of 7.1 m s^{-1} , yet *Stenella longirostris* individuals, swimming at a maximum swim speed of 6 m s^{-1} , about 15% slower than individuals of other species, achieve values of θ_R 2.5 to 21 times greater than the others. Of course, compared to *Megaptera* and *Balaenoptera* individuals, *Stenella* individuals have moments of inertia a few thousand times less, which certainly contributes to their subsurface performance. Still, *Stenella* individuals and those of *Tursiops* and *Lagenorhynchus* possess moments of inertia that vary only by factors of 4.8 down to 1.8, respectively. Yet both *Tursiops* and *Lagenorhynchus* possess rotational

performance ratios about 2.5 times smaller than *Stenella* individuals, implying that *Stenella* individuals can achieve greater flexions of their control surfaces compared to other dolphins.

Equation 6 embodies the physical condition for any animal in our model to be able to execute aerial spins from subsurface corkscrewing: the resistive torques on the pectoral flippers must exceed the sum of the resistive torques on all the other control surfaces. Thus, in the cases of *Megaptera* and *Balaenoptera*, smaller dorsal fins tend to enhance the ability to spin, but, as stated earlier, though the animal's ability to spin is enhanced, the number of spins executable is an interwoven function of the animal's moment of inertia, the sizes and placement of its control surfaces, its strength in powered motion, and its ability to regulate the flexions of its control surfaces. For *Megaptera* and *Balaenoptera*, their large moments of inertia are a primary limit to the number of executable aerial spins. From Table 1 we note that *Megaptera*'s moment of inertia is 11 times that of *Balaenoptera*, yet both whales are able to complete roughly one aerial spin (one for *Megaptera* and 0.76 for *Balaenoptera*). Consistent with our model, *Megaptera*'s performance is enhanced by its large, long flippers compared to *Balaenoptera*, as illustrated in Fig. 1.

Discussion

Various animals cross the air-water interface. They do this to escape predators (Gudger, 1944; Fish, 1990; Connor and Heithaus, 1996), capture food (Würsig and Würsig, 1980; Martin et al., 2005; Reys et al., 2009; Johnston et al., 2018; Würsig and Whitehead, 2018), circumvent obstacles (Lauritzen et al., 2001; Kondratieff and Myrick, 2006), reduce the energetics of swimming (Hui, 1987; Au and Weihs, 1980; Weihs, 2002; Würsig and Whitehead, 2018), take a breath (Hui, 1989), communicate (Würsig and Würsig, 1980; Whitehead, 1985; Félix, 2004; Lusseau, 2006; Dunlap et al., 2008, 2010; Kavanagh et al., 2016; Dudzinski and Gregg, 2018; Werth and Lemon, 2020), play (Whitehead, 1985; Würsig and Whitehead, 2018), provide aerial vision (Würsig and Würsig, 1980; Würsig and Whitehead, 2018), and dislodge parasites (Hester et al., 1963; Ritter, 2002; Ritter and Brunschweiler, 2003; Fish et al., 2006; Weihs et al., 2007). Animals that plunge dive into the water use gravity to accelerate downward in an aerial phase but hydrodynamically decelerate with penetration into the high density and viscosity medium, which limits the depth attained (Sharker et al., 2019). Alternatively, animals leaping from the water use

a high powered hydrodynamically dominated acceleration underwater to emerge into the air where a gravity dominated aerial phase is associated with a deceleration that limits leap height (Chang et al., 2019; Halsey and Iosilevskii, 2020). Cetaceans (whales and dolphins) generally cross the air-water interface to become completely airborne when breaching and porpoising (Whitehead, 1985; Au et al., 1988; Hui, 1989; Fish and Hui, 1991; Pearson, 2017; Aguilar and García-Vernet, 2018; Halsey and Iosilevskii, 2020; Segre et al., 2020; Werth and Lemon, 2020; Xia et al., 2021; Milmann et al., 2023; Serres et al., 2023; Yu et al., 2023).

Superimposed on the ability to cross the interface and leap from the water is the ability to spin while breaching. The motion of a cetacean performing spinning leaps is a combination of translational and rotational motion. The center of mass of the animal moves along a ballistic trajectory that is dependent on the escape angle and escape velocity. The start of the animal's rotation around its longitudinal axis occurs underwater (Fish et al., 2006). Rotation is produced by an imbalance between driving torques and resistive torques from the control surfaces. Upon breaching through the water surface with only the flukes in the water, the hydrodynamic torque and resistive torque of the pectoral flippers disappears, as does the resistive torque of the dorsal fin. The drive torque from the flukes, which is greater than the resistive torque of the flukes, produces a torque imbalance (Fish et al., 2006). By conservation of angular momentum, the torque imbalance produces an angular acceleration, which increases the animal's rate of spin as it emerges from the water.

For bodies using paired control surfaces, spinning or rolling results from these appendages producing an imbalance between each of the two wings, fins, or flippers. The imbalance is due to an asymmetrical pressure distributions and differential orientation of lift generation (Szurovy and Goulin, 1994; Segre et al., 2016; Fish and Lauder, 2017; Li et al., 2022). Such spinning maneuvers are used in aircraft acrobatics and military combat maneuvers as barrel-rolls and slow rolls (Gunston and Spick, 1988; Szurovy and Goulin, 1994). For cetaceans, body mass is directly associated with moment of inertia, and the flipper area is responsible for the lift generated to affect a spinning moment (Segre et al., 2016). The spinning is initiated underwater, where the asymmetrical fluid forces are large enough to destabilize the body in the roll axis. Once airborne, conservation of angular momentum dominates and the spin rate increases (Fish et al., 2006).

The spinner dolphins and spinner sharks perform such aerial spinning maneuvers to dislodge remoras (Fish et al., 2006; Weihs et al., 2007; Schwartz, 2013). Spinner dolphins are able to perform leaps with up to seven aerial spins (Fish et al. 2006) and an angular velocity of 4.6 Hz (F. Fish, per. obs.). For both dolphins and sharks, the ability to execute multiple spins with high angular velocities in the air is dependent on body morphology. These dolphins and sharks have slender body profiles that provide a low moment of inertia.

Moment of inertia is the rotational analog of an inertial mass. Moment of inertia depends on how the mass is distributed around the axis of rotation. With equivalent masses, a body with a large diameter will have greater rotational inertia and require a larger torque to start rotating than a more slender but longer body (Giancoli, 1991). The body shapes were similar with comparable fineness ratios of the other cetaceans examined, which would not ultimately affect the moment of inertia. Morphological differences affecting moment of inertia and thus spinning performance among the cetaceans were mainly mass, length, and girth. Small, slender dolphins (*Stenella*, *Lagenorhynchus* and *Tursiops*) displayed greater rates of spin than the larger baleen whales (*Balaenoptera* and *Megaptera*) with greater moments of inertia.

Though Eq. 6 and Eq. 9 were developed and tested with data from studies of cetaceans, those equations, along with Eq. 2, can apply to any similarly shaped aquatic animal, living or extinct. As was discussed in the Introduction, spinning behavior can serve multiple functions, functions (i.e., improved locomotion, maneuverability, play, dominance or aggressive display, alertness, acoustic communication, courtship display, dislodging ectoparasites), which are not restricted to cetaceans (Hester et al., 1963; Norris and Dohl, 1980; Norris et al., 1994; Fish et al., 2006; Weihs et al., 2007; Würsig and Whitehead, 2018). For example, remoras parasitize not only cetaceans, but sharks, too (Weihs et al., 2007; Schwartz, 2013). It is the expectation that the model can apply also to sharks known to execute aerial spins to rid themselves of attached remoras.

Differences in size affects performance for aquatic animals (Webb, 1975; Fish, 1998; Weber et al., 2014; Hirt et al., 2017; Gough et al., 2021; Segre et al., 2022). Although having similar densities, the combination of smaller mass and diameter for the spinner dolphin, *Stenella*, gives a moment of inertia that was only 56%, 21%, 0.05%, and 0.005% of *Lagenorhynchus*, *Tursiops*, *Balaenoptera*, and *Megaptera*, respectively (Table 1). The increase in size reduced the maximum ω_{SL} and number of aerial spins that could be accomplished (Table 1, 2). The large

whales (*Balaenoptera* and *Megaptera*) performed long-axis rolls prior to exiting the water. Whitehead (1985) noted that *Megaptera* twists while leaving the water. We measured rolling velocity for the large whales with tags with gyroscopes but were unable to directly video record the whales when breaching and spinning. However, the videos from on-board tags suggest that, when employed, rolling can be initiated at different times. With shallow trajectories, the roll is often initiated immediately before the whale breaks the surface of the water: the extended flippers rotate contra-laterally and the whale spins about its long axis. With deeper trajectories, the roll can be initiated much earlier. In both cases, the angular momentum continues the roll after the whale breaks the surface of the water (Fish et al., 2006).

Despite having a greater moment of inertia compared to *Balaenoptera*, *Megaptera* performed a maximum spin rate that was 2.3 times faster. The difference in spinning performance could be accounted for by the difference in flipper geometry. The flippers acting as control surfaces generate a lift force for the development of torque to initiate spinning underwater (Segre et al., 2016; Fish and Lauder, 2017). Members of the genus *Balaenoptera*, including the minke whale, use their flippers to roll at depth when targeting prey from below (Goldbogen et al., 2012; Segre et al., 2016). Maximum torque to spin is realized when one flipper generates a maximum upward lift and the other flippers generates a maximum downward lift (Segre et al., 2016). However, the dimensions of the flippers of *Balaenoptera* relative to the body size limits maneuvering performance (Weber et al., 2014). For a 14.4 m long fin whale (*Balaenoptera physalus*), the planar flipper area and length are 0.1195 m² and 1.48 m, respectively (Segre et al., 2016).

Comparatively, a 9.02 m long humpback whale (*Megaptera novaeangliae*) has a planar flipper area and length of 1.02 m² and 2.53 m, respectively (Fish and Battle, 1995). Fish and Battle (1995) found that although *Megaptera* was 37% shorter than *Balaenoptera physalus*, the *Megaptera* flipper had an area and length that was 88.3% and 41.5% larger, respectively, than for the *Balaenoptera physalus* flipper. *Megaptera* uses its elongate flippers to perform aquatic maneuvers underwater. These maneuvers consist of tightly banked turns during bubble feeding and somersaults (Jurasz and Jurasz, 1979; Fish and Battle, 1995). Maneuvering by *Megaptera* is also enhanced by the presence on the flipper of leading-edge tubercles that allow for the increased lift production and delay of stall when operating at high angles of attack (Miklosovic et

al., 2004; Fish et al., 2008; Fish, 2020). The geometry of the flipper of *Megaptera* would compensate for the whale's large moment of inertia.

Conclusion

The extraordinary leaps and aerial spins by cetaceans follow the fundamental laws of physics in regard to the moment of inertia and conservation of angular momentum. The rate at which each cetacean rotates about its longitudinal axis during aerial spinning leaps is dependent on the rate of spin underwater and the geometry of the body. The submerged spin rate is determined by the forces produced by the control surfaces that affect the whale's motion in roll prior to exiting the water. The large wing-like flippers of the humpback whale allow it to generate larger turning forces to perform greater spinning performance compared to a smaller whale. However in general, thin, small animals have higher rates of spin due to lower moments of inertia compared to large whales.

Acknowledgements

We greatly appreciate the cooperation of the trainers, staff, and dolphins at Sea World of Texas (San Antonio, TX) and the National Aquarium (Baltimore, MD). We appreciate the video of spinner dolphins supplied by the BBC with the cooperation of Ellen Husan, Grace Atkins, Doug Allan, Johnny Rogers, and Hugh Miller. We thank the assistance of Brandon Langston and Calista O'Brien for data collection. Data are available in the institutional data repository (http://digitalcommons.wcupa.edu/bio_data/9).

Competing interests

No competing interests are declared by the authors.

Author contributions

F.E.F was the primary author for the study. J.A.G. and F.E.F. obtained funding for the study. A.J.N. developed the equations for the analysis of spinning. K.L.C., W.T.G., S.R.K-R and P.S.S. were involved with video recording and analysis and collecting morphometric data. J.St.L. provided logistical support involved with video recording of captive species.

Funding

This research was supported by grants from the National Science Foundation (IOS-1656676) to J.A.Goldbogen, J. Potvin, and F.E.Fish and the Office of Naval Research (N000141410533) to F.E.Fish.

Key

A	Area of control surface (m^2)
C	Drag coefficient
CG	Center of gravity
D	Body diameter (m)
F	Force ($\text{N} = \text{kg m s}^{-2}$)
g	Gravitational acceleration (9.8 m s^{-2})
I	Moment of inertia (kg m^2)
k_1	Added mass coefficient
L	Body length (m)
M	Body mass (kg)
N	Number of complete spins
R	Maximum radius of body (m)
R_P	Conformation constant for pectoral flippers ($\text{kg m}^2 \text{ rad}^{-2}$)
R_D	Conformation constant for dorsal fin ($\text{kg m}^2 \text{ rad}^{-2}$)
R_F	Conformation constant for caudal flippers ($\text{kg m}^2 \text{ rad}^{-2}$)
Δx	Distance between control surfaces (m)
θ_R	Rotational performance coefficient (rad m^{-1} , deg m^{-1})
ρ	Density of sea water (1025 kg m^{-3})

τ	Torque (N m)
v_s	Swimming speed (m s^{-1})
ω_A	Angular speed of spinning underwater (deg s^{-1} , rad s^{-1})
ω_{sl}	Maximum rate of aerial spin leaps (deg s^{-1} , rad s^{-1})

References

- Aguilar, A. and García-Vernet, R.** (2018). Fin Whale: *Balaenoptera physalus*. In *Encyclopedia of Marine Mammals Ed. 3* (ed. B. Würsig, J.G.M. Thewissen and K.M. Kovaks), pp. 368–371. London: Academic Press.
- Au, D. and Weihs, D.** (1980). At high speeds dolphins save energy by leaping. *Nature* **284**, 548-550.
- Au, D., Scott, M.D. and Perryman, W.L.** (1988). Leap-swim behavior of ‘porpoising’ dolphins. *Cetus* **8**, 7-10.
- Cade, D.E., Barr, K.R., Calambokidis, J., Friedlaender, A.S. and Goldbogen, J.A.** (2018). Determining forward speed from accelerometer jiggle in aquatic environments. *Journal of Experimental Biology* **221**, jeb170449.
- Chang, B., Myeong, J. Viro, E., Clanet, C., Kim, H-Y. and Jung, S.** (2019). Jumping dynamics of aquatic animals. *Journal of the Royal Society Interface* **16**, 20190014.
- Cheneval, O., Blake, R.W., Trites, A.W. and Chan K.H.S.** (2007). Turning maneuvers in Steller sea lions (*Eumatopias jubatus*) *Marine Mammal Science* **23**, 94-109.
- Connor, R.C. and Heithaus, M.R.** (1996). Approach by great white shark elicits flight response in bottlenose dolphins. *Marine Mammal Science* **12**, 602-606.
- Domenici, P. and Blake, R.W.** (1997). The kinematics and performance of fish fast-start swimming. *Journal of Experimental Biology* **200**, 1165-1178.

- Downs, A.M., Kolpas, A., Block, B.A. and Fish, F.E.** (2023). Multiple behaviors for turning performance of Pacific bluefin tuna (*Thunnus orientalis*). *Journal of Experimental Biology* **226**, jeb244144. doi:10.1242/jeb244144.
- Dudzinski, K.M. and Gregg, J.D.** (2018). Communication. In *Encyclopedia of Marine Mammals Ed. 3* (ed. B. Würsig, J.G.M. Thewissen and K.M. Kovaks), pp. 210–215. London: Academic Press.
- Dunlop, R.A., Cato, D.H. and Noad, M.J.** (2008). Non-song acoustic communication in migrating humpback whales (*Megaptera novaeangliae*). *Marine Mammal Science* **24**, 613-629.
- Dunlop, R.A., Cato, D.H. and Noad, M.J.** (2010). Your attention please: increasing ambient noise levels elicits a change in communication behaviour in humpback whales (*Megaptera novaeangliae*). *Proceedings of the Royal Society B: Biological Sciences* **277**, 2521-2529.
- Félix, F.** (2004). Assessment of the level of surface activity in humpback whales during the breeding season. *Latin American Journal of Aquatic Mammals* **3**, 25-36.
- Fish, F.E.** (1990). Wing design and scaling of flying fish with regard to flight performance. *Journal of Zoology, London* **221**, 391-403.
- Fish, F.E.** (1998). Comparative kinematics and hydrodynamics of odontocete cetaceans: Morphological and ecological correlates with swimming performance. *Journal of Experimental Biology* **201**, 2867-2877.
- Fish, F.E.** (2002). Balancing requirements for stability and maneuverability in cetaceans. *Integrative and Comparative Biology* **42**, 85-93. doi:10.1093/icb/42.1.85
- Fish, F.E. and Hui, C.A.** (1991). Dolphin swimming: A review. *Mammal Review* **21**, 181-196.
- Fish, F.E. and Battle, J.M.** (1995). Hydrodynamic design of the humpback whale flipper. *Journal of Morphology* **225**, 51–60.
- Fish, F. E.** (2020). Biomimetics and the application of the leading edge tubercles of the humpback whale flipper. In *Flow Control through Bio-Inspired Leading Edge Tubercles* (ed. D.T.H. New and B.F. Ng). pp. 1-39. Cham, Switzerland: Springer.

- Fish, F.E., Hurley, J. and Costa, D.P.** (2003). Maneuverability by the sea lion, *Zalophus californianus*: Turning performance of an unstable body design. *Journal of Experimental Biology* **206**, 667-674. doi:10.1242/jeb.00144
- Fish, F.E. and Nicastrò, A.J.** (2003). Aquatic turning performance by the whirligig beetle: constraints on maneuverability by a rigid biological system. *Journal of Experimental Biology* **206**, 1649-1656. doi:10.1242/jeb.00305
- Fish, F. E., Nicastrò, A.J. and Weihs, D.** (2006). Dynamics of the aerial maneuvers of spinner dolphins. *Journal of Experimental Biology* **209**, 590-598.
- Fish, F.E., Bostic, S.A. Nicastrò, A.J., and Beneski, J.T.** (2007). Death roll of the alligator: mechanics of twist feeding in water. *Journal of Experimental Biology* **210**, 2811-2818.
- Fish, F. E., Howle, L. E. and Murray, M. M.** (2008). Hydrodynamic flow control in marine mammals. *Integrative and Comparative Biology* **211**, 1859-1867.
- Fish, F.E. and Lauder, G.V.** (2017). Control surfaces of aquatic vertebrates in relation to swimming modes. *Journal of Experimental Biology* **220**, 4351-4363. doi:10.1242/jeb.149617
- Fish, F.E. and Holzman, R.** (2019). Swimming turned on its head: Stability and maneuverability of the shrimpfish (*Aeoliscus punctulatus*). *Integrative Organismal Biology* **55**, E57-E57.
- Giancoli, D.C.** (1991). *Physics*. Englewood Cliffs, NJ: Prentice Hall.
- Goldbogen, J.A., Calambokidis, J., Friedlaender, A.S., Francis, J., DeRuiter, S.L., Stimpert, A.K., Falcone, E. and Southall, B.L.** (2013). Underwater acrobatics by the world's largest predator: 360 rolling manoeuvres by lunge-feeding blue whales. *Biology Letters* **9**, 20120986.

- Gough, W.T., Segre, P.S., Bierlich, K.C., Cade, D.E., Potvin J., Fish, F.E., Dale, J., di Clemente, J., Friedlaender, A.S., Johnston, D.W., Kahane-Rapport, S.R., Kennedy, J., Long, J.H., Oudejans, M., Penry, G., Savoca, M.S., Simon, K.A., Visser, F., Wiley, D.N. and Goldbogen, J.A.** (2019). Scaling of swimming performance in baleen whales. *Journal of Experimental Biology* **222**, jeb.204172.
- Gough, W. T., Smith, H., Savoca, M., Czapanskiy, M., Fish, F., Potvin, J., Bierlich, K. C., Cade, D., Di Clemente, Kennedy, J., Segre, P., Stanworth. A., Weir, C. and Goldbogen, J. A.** (2021). Scaling of oscillatory kinematics and Froude efficiency in baleen whales. *Journal of Experimental Biology* **224**, jeb237586.
- Gudger, E.W.** (1944). Fishes that play “leapfrog”. *American Naturalist* **78**, 451-463.
doi.org/10.1086/281216
- Gunston, B. and Spick, M.** (1988). *Modern Air Combat: The Aircraft, Tactics and Weapons Employed in Aerial Warfare Today*. New York: Crescent.
- Halsey, L.G. and Iosilevskii, G.** (2020). The energetics of ‘airtime’: estimating swim power from breaching behaviour in fishes and cetaceans. *Journal of Experimental Biology* **223**, jeb216036.
- Harris, J.E.** (1936). The role of the fins in the equilibrium of the swimming fish. I. Wind-tunnel tests on a model of *Mustelus canis* (Mitchill). *Journal of Experimental Biology* **13**, 476-493.
- Harris, J.E.** (1937). The mechanical significance of the position and movements of the paired fins in the Teleostei. *Papers from Tortugas Laboratory* **31**, 173-189.
- Helfman, G.S. and Clark, J.B.** (1986). Rotational feeding: overcoming gape- limited foraging in anguillid eels. *Copeia* **1986**, 679-685.
- Hester, F. J., Hunter, J. R. and Whitney, R. R.** (1963). Jumping and spinning behavior in the spinner porpoise. *Journal of Mammalogy* **44**, 586-588.

- Hirt, M.R., Jetz, W., Rall, B.C. and Brose, U.** (2017). A general scaling law reveals why the largest animals are not the fastest. *Nature Ecology & Evolution* **1**, 1116-1122.
- Howland, H.C.** (1974). Optimal strategies for predator avoidance: The relative importance of speed and manoeuvrability. *Journal of Theoretical Biology* **47**, 333-350.
- Hui, C.A.** (1987). The porpoising of penguins: an energy-conserving behavior for respiratory ventilation. *Canadian Journal of Zoology* **65**, 209-211.
- Hui, C.A.** (1989). Surfacing behavior and ventilation in free-ranging dolphins. *Journal of Mammalogy* **70**, 833-835.
- Johnston, E.M., Halsey, L.G., Payne, N.L., Kock, A.A., Iosilevskii, G., Whelan, B. and Houghton, J. D. R.** (2018). Latent power of basking sharks revealed by exceptional breaching events. *Biology Letters* **14**, 20180537.
- Jurasz, C. M. and Jurasz, V. P.** (1979). Feeding modes of the humpback whale, *Megaptera novaeangliae*, in southeast Alaska. *Scientific Reports of the Whales Research Institute* **31**, 69-83.
- Kahane-Rapport, S. R. and Goldbogen, J. A.** (2018). Allometric scaling of morphology and engulfment capacity in rorqual whales. *Journal of Morphology* **279**, 1256-1268.
- Kavanagh, A. S., Owen, K., Williamson, M. J., Blomberg, S. P., Noad, M. J., Goldizen, A. W., Kniest, E., Cato, D. H. and Dunlop, R. A.** (2017). Evidence for the functions of surface-active behaviors in humpback whales (*Megaptera novaeangliae*). *Marine Mammal Science* **33**, 313-334.
- Kondratieff, M.C. and Myrick, C.A.** (2006). How high can brook trout jump? A laboratory evaluation of brook trout jumping performance. *Transactions of the American Fisheries Society* **135**, 361–370.
- Lamb, H.** (1932). Hydrodynamics. Cambridge: Cambridge University Press.
- Lauritzen, D.V., Hertel, F. and Gordon, M.S.** (2001). Experimental studies of jumping preferences of adult migrating Pacific salmon. *American Zoologist* **41**, 1502– 1503.

- Leahy, A. M., Fish, F. E., Kerr, S. J., Zeligs, J. A., Skrovan, S., Cardenas, K. L. and Leftwich, M. C.** (2021). The role of California sea lion (*Zalophus californianus*) hindflippers as aquatic control surfaces for maneuverability. *Journal of Experimental Biology* **224**: jeb243020.
- Li, Z., Xia, D., Zhou, ., Cao, J., Chen, Weishan and Wang, X.** (2022). The hydrodynamics of self-rolling locomotion driven by the flexible pectoral fins of a 3-D bionic dolphin. *Journal of Ocean Engineering and Science* **7**, 29-40.
- Lissaman, P.** (2007). Fundamentals of energy extraction from natural winds. *Technical Soaring* **31**, 36-41.
- Lockyer, C.** (1976). Body weights of some species of large whales. *Journal du Conseil International pour l'Exploration de la Mer* **36**, 259-273.
- Lusseau, D.** (2006). Why do dolphins jump? Interpreting the behavioural repertoire of bottle nose dolphins (*Tursiops* sp.) in Doubtful Sound, New Zealand. *Behavioural Processes* **73**, 257-265.
- Martin, R.A., Hammerschlag, N., Collier, R.S. and Fallows, C.** (2005). Predatory behaviour of white sharks (*Carcharodon carcharias*) at Seal Island, South Africa. *JMBA-Journal of the Marine Biological Association of the United Kingdom* **85**, 1121-1136.
- Miklosovic, D.S., Murray, M.M., Howle, L.E. and Fish, F.E.** (2004). Leading-edge tubercles delay stall on humpback whale (*Megaptera novaeangliae*) flippers. *Physics of Fluids* **16**, L39-L42.
- Milmann, L., Cardoso, J., Francisco, A., Santos, F.P., Seminara, C., Abras, D.R., Marques, M.L., Hille, D.A., Lemos, L.S., Ruenes, G.F. and Hauser-Davis, R.A.** (2023). Dwarf minke whale (*Balaenoptera acutorostrata* subsp.) interactions with vessels off the coast of Brazil. *Cetacean Population Studies* 2022S002.
- Norris, K.S. and Dohl, T.P.** (1980). Behavior of the Hawaiian spinner dolphin, *Stenella longirostris*. *Fisheries Bulletin* **77**, 821-849.

- Norris, K.S., Würsig, B., Wells, R. S. and Würsig, M.** (1994). The Hawaiian Spinner Dolphin. Berkeley: University of California Press.
- Nowak R.M.** (1999). *Walker's Mammals of the World*. Baltimore: John's Hopkins University Press.
- Pearson, H.C.** (2017). Unravelling the function of dolphin leaps using the dusky dolphin (*Lagenorhynchus obscurus*) as a model species. *Behaviour* **154**, 563-581.
- Perrin, W.F. and Gilpatrick, J.W., Jr** (1994). Spinner dolphin *Stenella longirostris* (Gray, 1828). In Handbook of Marine Mammals, Vol. 5, The First Book of Dolphins (ed. S.H. Ridgway and R. Harrison), pp. 99-128. San Diego: Academic Press.
- Potter, M.C. and Foss, J.F.** (1975). *Fluid Mechanics*. New York: Ronald Press.
- Reys, P., Sabino, J. and Galetti, M.** (2009). Frugivory by the fish *Brycon hilarii* (Characidae) in western Brazil. *Acta Oecologica* **35**, 136-141.
- Ritter, E. K.** (2002). Analysis of sharksucker, *Echeneis naucrates*, induced behavior patterns in the blacktip shark, *Carcharhinus limbatus*. *Environmental Biology of Fishes* **65**, 111-115.
- Ritter, E.K. and Brunschweiler, J.M.** (2003). Do sharksuckers, *Echeneis naucrates*, induce jump behaviour in blacktip sharks, *Carcharhinus limbatus*? *Marine and Freshwater Behaviour and Physiology* **36**, 111-113.
- Schwartz, F.J.** (2013). Jumping and spinning by carcharhinid sharks another view. *Journal of the North Carolina Academy of Science* **129**, 107-110.
- Segre, P.S., Cade, D.E., Fish, F.E., Allen, A.N., Calambokidis, J., Friedlander, A.S. and Goldbogen, J.A.** (2016). Hydrodynamic properties of fin whale flippers predict rolling performance. *Journal of Experimental Biology* **219**, 3315-3320.
- Segre, P.S., Cade, D.E., Calambokidis, J., Fish, F.E., Friedlaender, A.S., Potvin, J. and Goldbogen, J.A.** (2018). Body flexibility enhances maneuverability in the world's largest predator. *Integrative and Comparative Biology* **59**, 1-13.

- Segre, P.S., Potvin, J., Cade, D.E., Calambokidis, J., Di Clemente, J., Fish, F.E., Friedlaender, A.S., Gough, W.T., Kahane-Rapport, S.R., Oliveria, C. Parks, S.E., Penry, G.S., Simon, M., Stimpert, A.K., Wiley, D.N., Bierlich, K.C., Madsen, P.T. and Goldbogen, J.A. (2020). Energetic and physical limitations on the breaching performance of large whales. *eLife* **9**, e51760.
- Segre, P. S., Gough, W. T., Roualdes, E. A., Cade, D. E., Czapanskiy, M. F., Fahlbush, J., Kahane-Rapport, S. R., Oestreich, W. K., Bejder, L., Bierlich, K. C., Burrows, J. A., Calambokidis, J., Chenoweth, E. M., di Clemente, J., Durban J. W., Fearnbach, H., Fish, F. E., Friedlaender, A. S., Hegelund, P., Johnston, D. W., Nowacek, D. P., Oudejans, M., Penry, G. S., Potvin, J., Simon, M., Stanworth, A., Straley, J. M., Szabo, A., Videsen, S. K. A., Visser, F., Weir, C. R., Wiley, D. N. and Goldbogen, J. A. (2022). Scaling of maneuvering performance in baleen whales: larger whales outperform expectations. *Journal of Experimental Biology* **225**, jeb243224.
- Serres, A., Lin, W., Liu, B., Chen, S. and Li, S. (2023). Context of breaching and tail slapping in Indo-Pacific humpback dolphins in the northern South China Sea. *Behavioral Ecology and Sociobiology* **77**, 64.
- Sharker, S.I., Holekamp, S., Mansoor, M.M., Fish, F.E. and Truscott, T. (2019). Water entry impact dynamics of diving birds. *Bioinspiration & Biomimetics* **14**, 56013-56013.
- Szurovy, G. and Goulian, M. (1994). *Basic Aerobatics*. New York: Tab Books.
- Webb, P.W. (1975). Hydrodynamics and energetics of fish propulsion. *Bulletin of the Fisheries Research Board of Canada* **190**, 1-159.
- Webb, P.W. (1983). Speed, acceleration and manoeuvrability of two teleost fishes *Journal of Experimental Biology* **102**, 115-122.
- Webb, P.W. (1984). Form and function in fish swimming. *Scientific American* **251**, 72-82.
- Webb, P.W. (2004). Maneuverability-General Issues. *Journal of Oceanic Engineering* **29**, 547-555.
- Webb, P.W. (2006). Stability and maneuverability. In *Fish Physiology: Fish Biomechanics*, Vol. 23 (ed. R.E. Shadwick and G.V. Lauder), p. 281-332. Amsterdam: Academic Press.

- Weber, P.W., Howle, L.E., Murray, M.M., Reidenberg, J.S. and Fish, F.E.** (2014). Hydrodynamic performance of the flippers of large-bodied cetaceans in relation to locomotor ecology. *Marine Mammal Science* **30**, 413-432.
- Wei, C., Houser, D., Erbe, C., Matrai, E. and Ketten, D. R.** (2023). Does rotation increase the acoustic field of view? Comparative models based on CT data of a live dolphin versus a dead dolphin. *Bioinspiration & Biomimetics* **18**, 035006.
- Weihs, D.** (2002). Dynamics of dolphin porpoising revisited. *Integrative and Comparative Biology* **42**, 1071-1078.
- Weihs, D., Fish, F.E. and Nicastrò, A.J.** (2007). Mechanics of remora removal by dolphin spinning. *Marine Mammal Science* **23**, 707-714.
- Werth, A.J. and Lemon, C.L.** (2020). Whale breaching says it loud and clear. *eLife* **9**, e55722.
- Whitehead, H.** (1985). Humpback whale breaching. *Investigations on Cetaceans* **17**, 117-156.
- Wiley, D., Ware, C., Bocconcelli, A., Cholewiak, D., Friedlaender, A., Thompson, M. and Weinrich, M.** (2011). Underwater components of humpback whale bubble-net feeding behaviour. *Behaviour* **148**, 575-602.
- Würsig, B. and Würsig, M.** (1980). Behavior and ecology of the dusky dolphin, *Lagenorhynchus obscurus*, in the South Atlantic. *Fisheries Bulletin* **77**, 871-890.
- Würsig, B., Dorsey, E.M., Richardson, W.J. and Wells, R.S.** (1989). Feeding, aerial and play behaviour of the bowhead whale, *Balaena mysticetus*, summering in the Beaufort Sea. *Aquatic Mammals* **15**, 27-37.
- Würsig, B., and Whitehead, H.** (2018). Aerial behavior. In *Encyclopedia of Marine Mammals*, Ed. 3. (ed. W.F. Perrin, B. Würsig, and J.G.M. Thewissen), pp. 6-10. London: Academic Press.
- Xia, D., Yin, Q., Li, Z., Chen, W., Shi, Y. and Dou, J.** (2021). Numerical study on the hydrodynamics of porpoising behavior in dolphins. *Ocean Engineering*, **229**, 108985.
- Yu, J., Wang, T., Chen, D. and Meng, Y.** (2023). Quantifying the leaping motion using a self-propelled bionic robotic dolphin platform. *Biomimetics* **8**, 21.

Figures

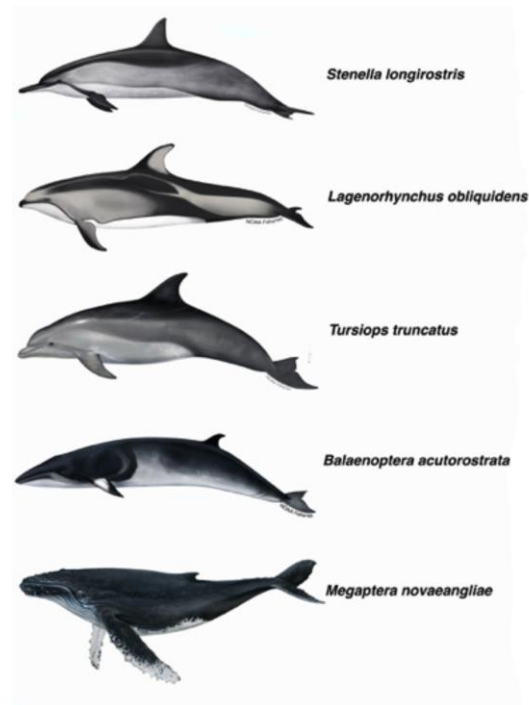
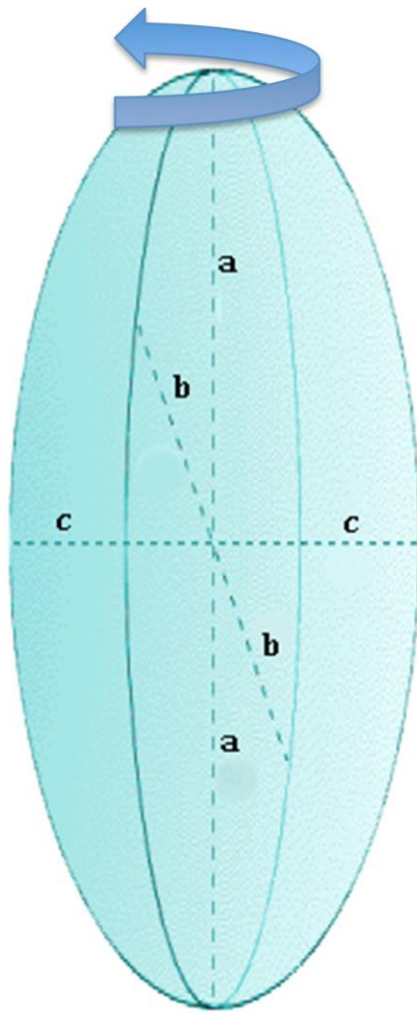


Fig. 1. Comparative body shapes of cetaceans examined. Images are arranged with respect to body mass from lowest to highest. Images are not drawn to scale.



$$I = (2MR^2)/5$$

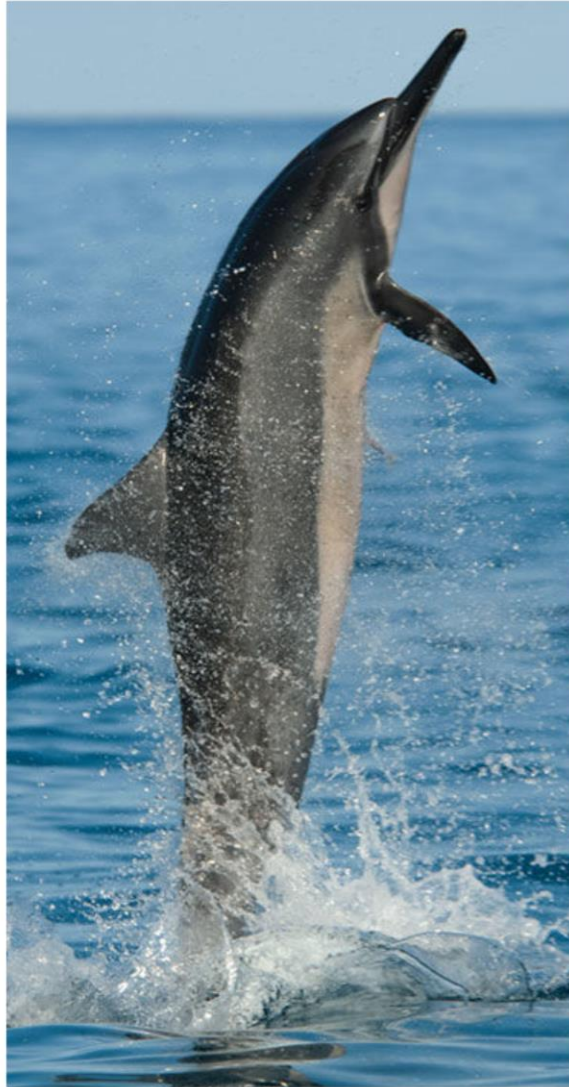


Fig. 2. Prolate spheroid and spinner dolphin (*Stenella longirostris*). The dimension a was equivalent to the total body length. Dimensions b and c were equal and assumed to be equivalent to the maximum diameter of the cetacean. The equation for the moment of inertia (I) for the prolate spheroid is provided, where M is the body mass plus the added mass of the entrained water and R is the maximum radius of the body without the control surfaces.

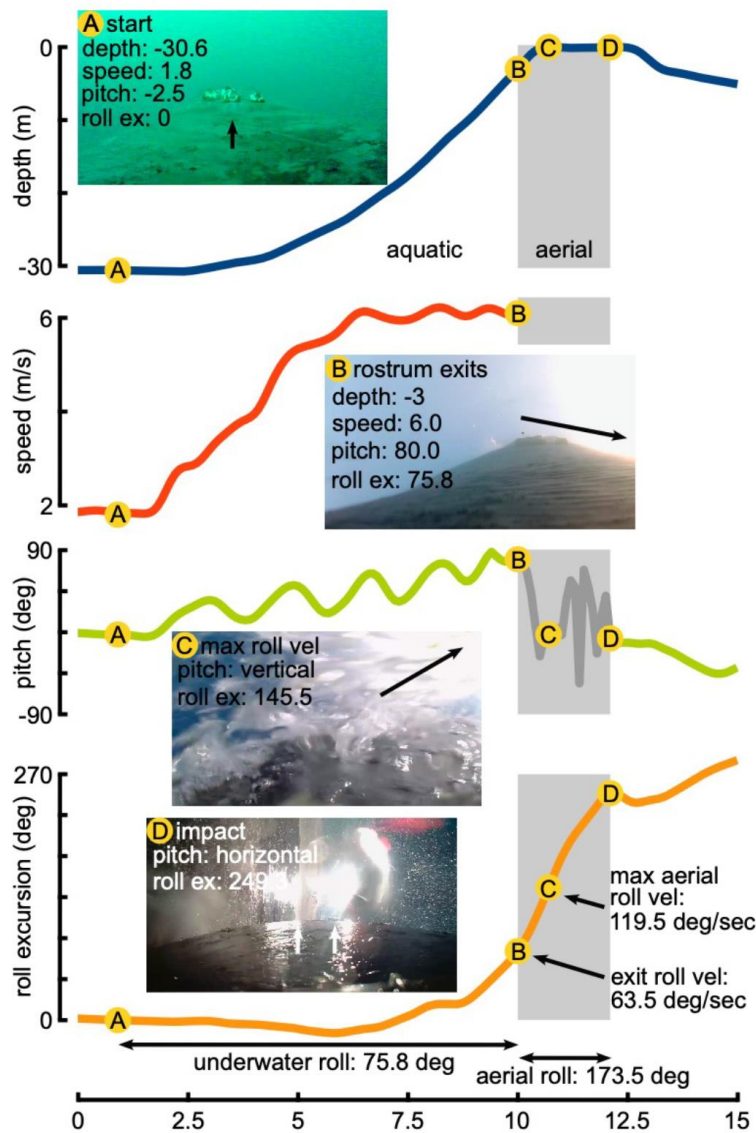


Fig. 3. Spinning performance of a humpback whale during a breach. Biologging sensors measured depth (blue), speed (red), pitch (green), and the roll (orange) was measured using the gyroscope parallel to the axis of the long-axis of the body. Using the gyroscopes (as opposed to accelerometer-derived roll) allows for the measurement of roll when the whale is near vertical. Photos from the onboard cameras are shown as the whale begins its acceleration (A), as the rostrum emerges from the water (B), at the moment of the highest roll velocity (C) and as the whale hits the water and rolling stops (D). The arrows highlight different features of the whale and the environment, which act as a visual confirmation of the roll. Note, the speed measurement

only works while the tag is underwater and therefore is not shown after the rostrum breaks the surface. Similarly, the accelerometer-derived pitch has a high level of error when the whale is out of the water (shaded) and should be interpreted with caution during this time. A video of this breach can be found in the supplementary material.

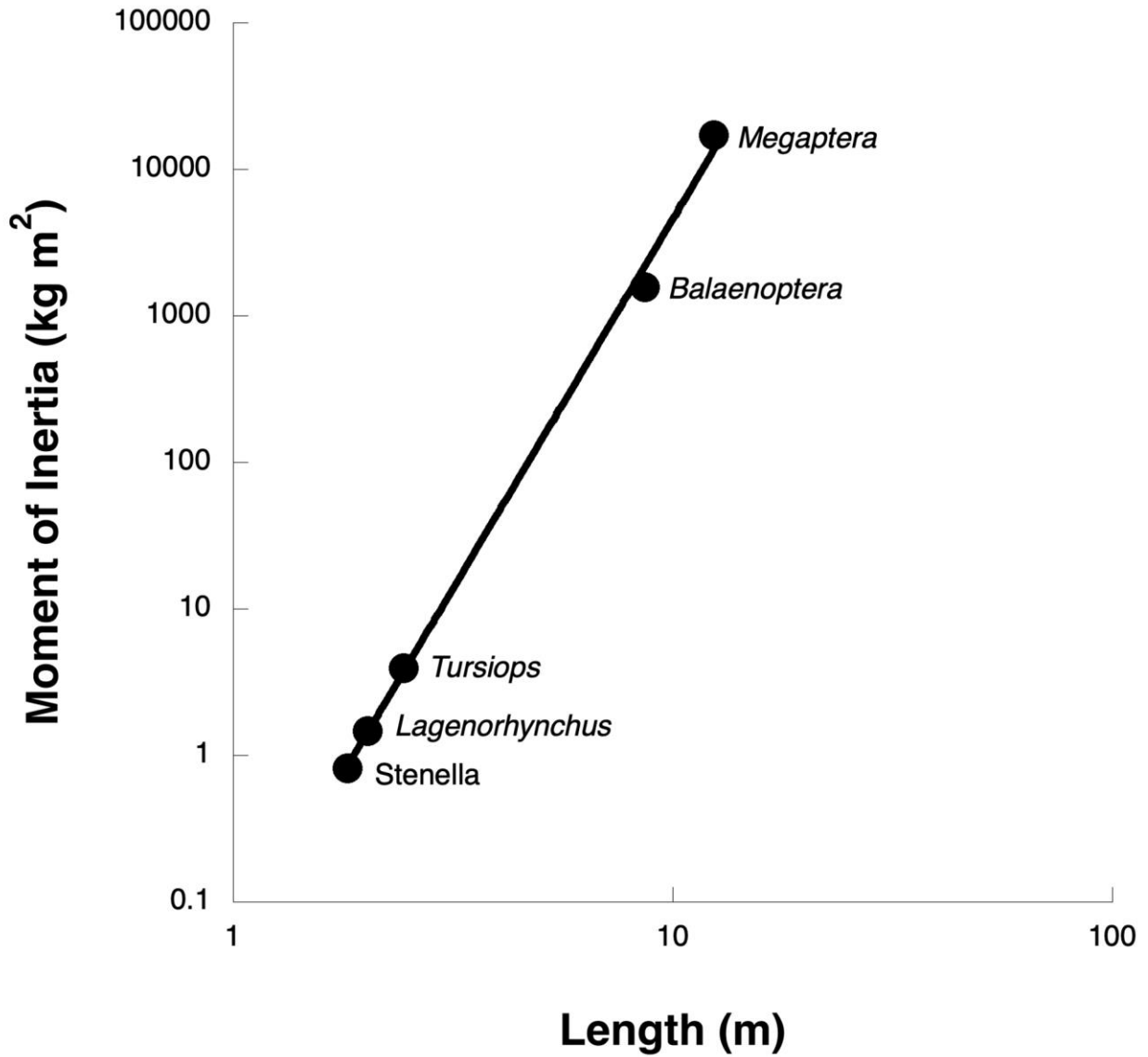


Fig. 4. Relationship between body length (L) and the moment of Inertia (I). This relationship was expressed by the equation $I = 0.041 L^{5.043}$ with a correlation coefficient of $r = 0.997$. Data are plotted on a logarithmic scale.

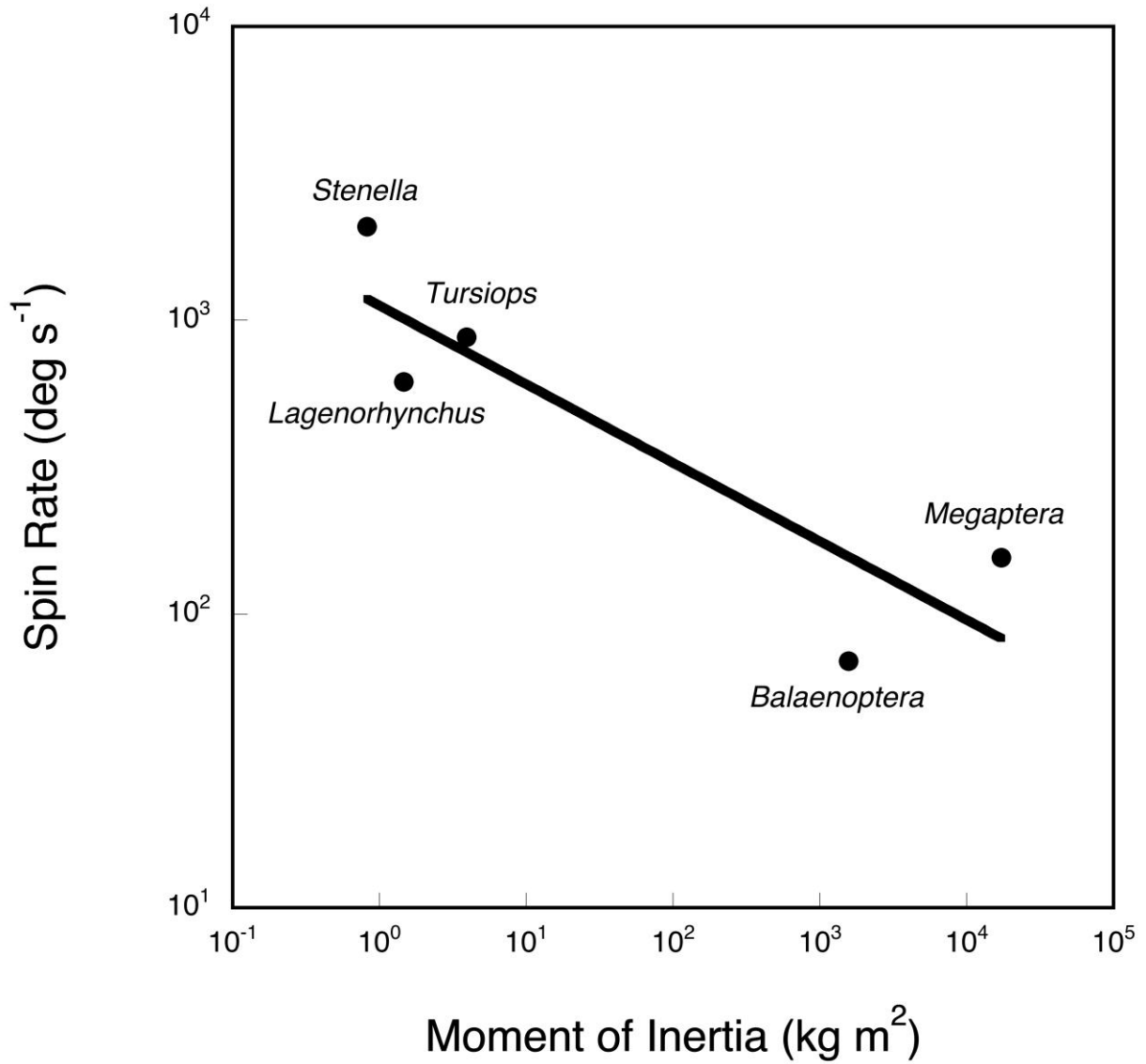


Fig. 5. The maximum rate of aerial spins (ω_{SL}) with respect to the moment of Inertia (I). The relationship was expressed by the regression equation $I = 1123.6 L^{-0.268}$ with a correlation coefficient of $r = 0.835$. Data are plotted on a logarithmic scale.

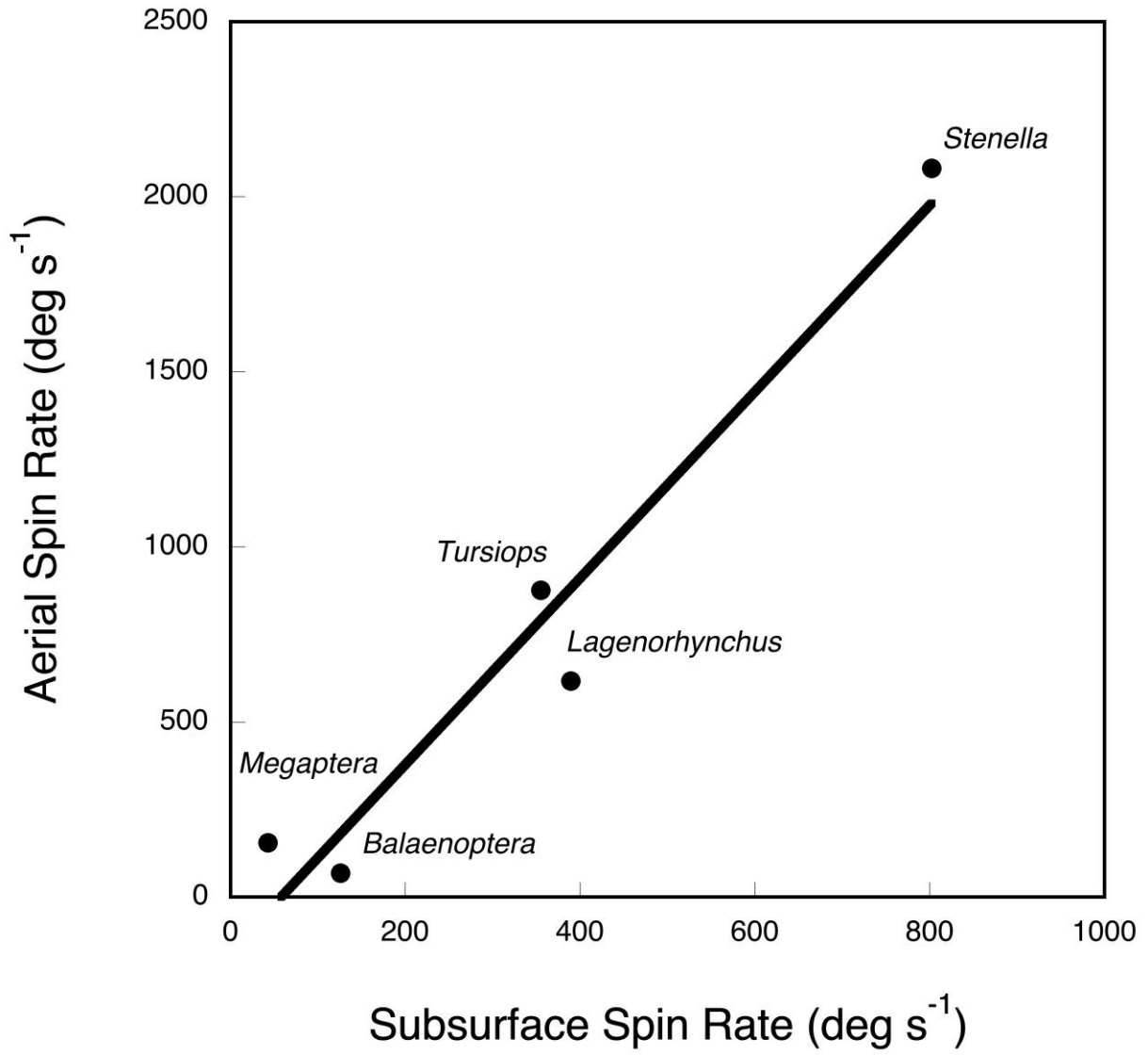


Fig. 6. Aerial spin rate versus subsurface spin rate.

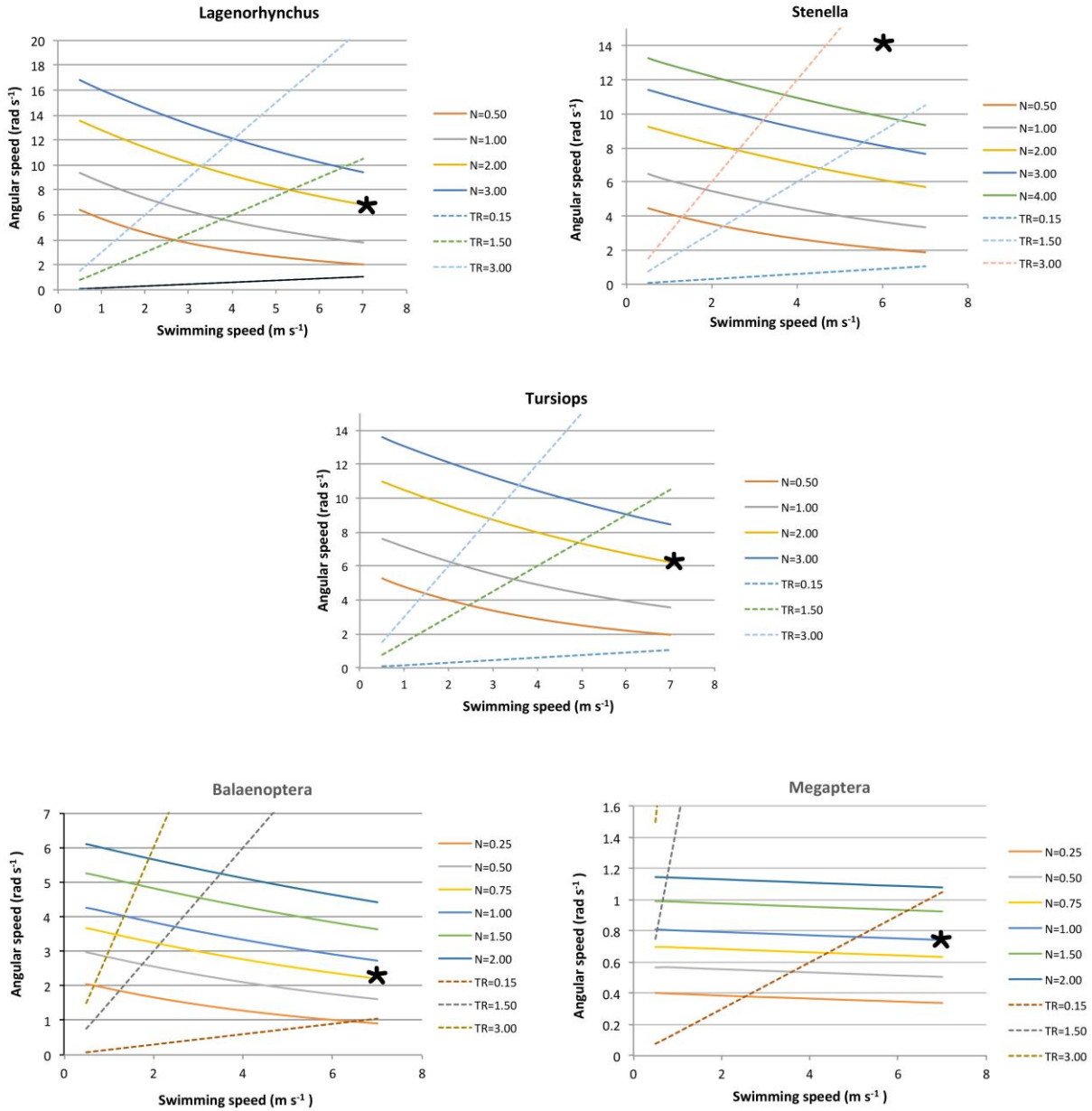


Fig. 7. Relationship between the angular speed (ω_A) while swimming underwater necessary to execute various numbers of complete spins (N ; solid lines) over a range of swimming speed (v_S). As a basis for comparison among the five species studied, the three dashed diagonal lines represent three values of the subsurface rotational performance coefficient, θ_R (in rad m^{-1}), defined to be the ratio of ω_A/v_S . TR in the legend represents θ_R . The stars indicate the actual performance for each species studied, that is, the maximum number of spins observed

corresponding to an animal's maximum swim speed. For example, for a *Lagenorhynchus* individual, whose maximum swim speed is 7.3 m s^{-1} , a maximum of $N=2$ spins were observed (yellow curved, solid line). The corresponding rotational performance coefficient is between 0.15 and 1.5 rad m^{-1} , but can be computed more precisely using our model; those values appear in Table 2. For *Lagenorhynchus*, $\theta_R = 0.93 \text{ rad m}^{-1}$, equivalent to 53 degrees per meter of subsurface travel. The solid, curved lines in each graph are computed from Eq. 1 using morphometric data from measurements of individuals of each species. Once the dimensions of the body, the dimensions and location of the control surfaces, and the total mass are measured, the individual's moment of inertia can be determined. Thus, for a particular swim speed, v_S , the theoretical subsurface rotation rate, ω_A , can be determined which generates N spins. The observed maximum number of spins sets the rotational performance limit of each species.

Table 1. Body dimensions, moment of Inertia, and maximum spin rates for leaping cetaceans.

Species	Length m	Radius m	Fineness Ratio	Mass + Added Mass kg	Moment of Inertia kg m ²	Max Spin Rate deg s ⁻¹	Max Spin Rate rad s ⁻¹
<i>Balaenoptera acutorostrata</i>	8.64	0.69	6.3	8373.0	1571.5	69	1.0
<i>Lagenorhynchus obliquidens</i>	2.02	0.20	5.0	91.3	1.5	618	10.8
<i>Megaptera novaeangliae</i>	12.40	1.19	5.2	30488.0	17211.6	156	1.5
<i>Stenella longirostris</i>	1.82	0.17	5.3	68.8	0.8	2081	36.3
<i>Tursiops truncatus</i>	2.44	0.24	5.2	176.3	3.9	877	15.3

Table 2. Aerial spinning performance of cetaceans. For various cetaceans studied, this table lists the maximum observed swimming speed, v_S , and the maximum number of observed aerial spins. From this information and the predictions of our model in the graphs, the maximum angular subsurface speed, ω_A is found and consequently, the maximum value of the rotational performance coefficient, θ_R . Values of ω_A and θ_R are given in rad s^{-1} and rad m^{-1} with values in parentheses of deg s^{-1} and deg m^{-1} , respectively.

Species	v_S m s^{-1}	N (maximum)	ω_A rad s^{-1} (deg s^{-1})	θ_R rad m^{-1} (deg m^{-1})
<i>Balaenoptera acutorostrata</i>	7.1	0.76	2.2 (126.1)	0.31 (17.8)
<i>Lagenorhynchus obliquidens</i>	7.3	2	6.8 (389.6)	0.93 (53.3)
<i>Megaptera novaeangliae</i>	7.0	1	0.75 (43.0)	0.11 (6.3)
<i>Stenella longirostris</i>	6.0	7	14.0 (802.1)	2.30 (131.8)
<i>Tursiops truncatus</i>	7.1	2	6.2 (355.2)	0.87 (49.8)

40 Ton Humpback Whale Leaps Entirely Out of the Water! A Video by Craig Capehart

<https://www.youtube.com/watch?v=fhflpUgxgm8>

2013 Humpback Breach from Underwater Jones

<https://www.youtube.com/watch?v=x6wZJ59nyqw>

A Humpback Whale Breaches in Tofino, B.C. and Performs a Full 360-Degree Spin

<https://www.youtube.com/watch?v=vpCv9-SfnxI>

Active Breaching Humpbacks: Mother "Big Momma" and her calf

<https://www.youtube.com/watch?v=zdlrnMbx0o0>

Incredible Humpback Whale Breach

<https://www.youtube.com/watch?v=7NAKaSo19us>

UNSEEN_ Whale breach near miss with swimmer

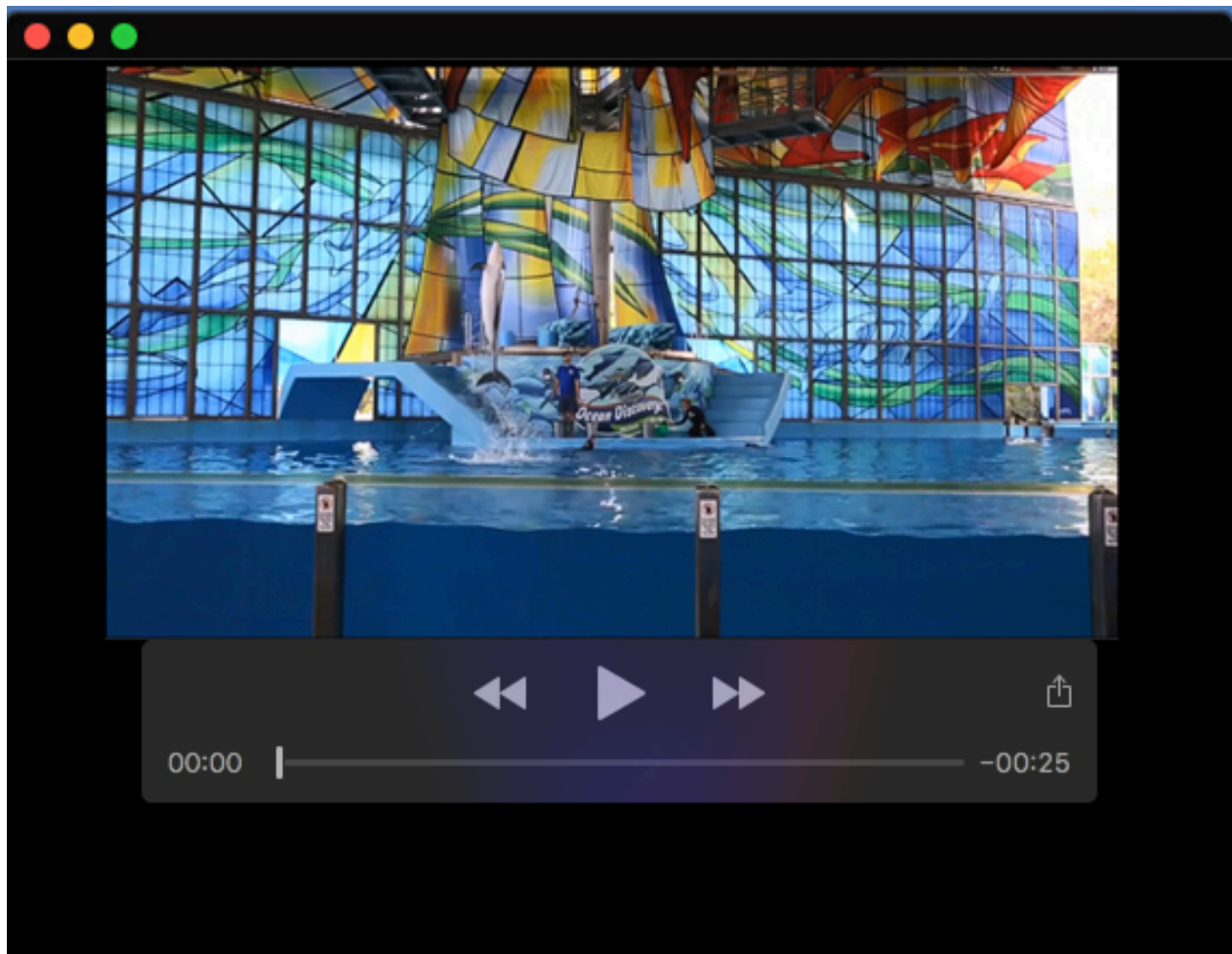
<https://www.youtube.com/watch?v=A7ZON5ztSsc>

Whale jumps out of nowhere during sight seeing tour

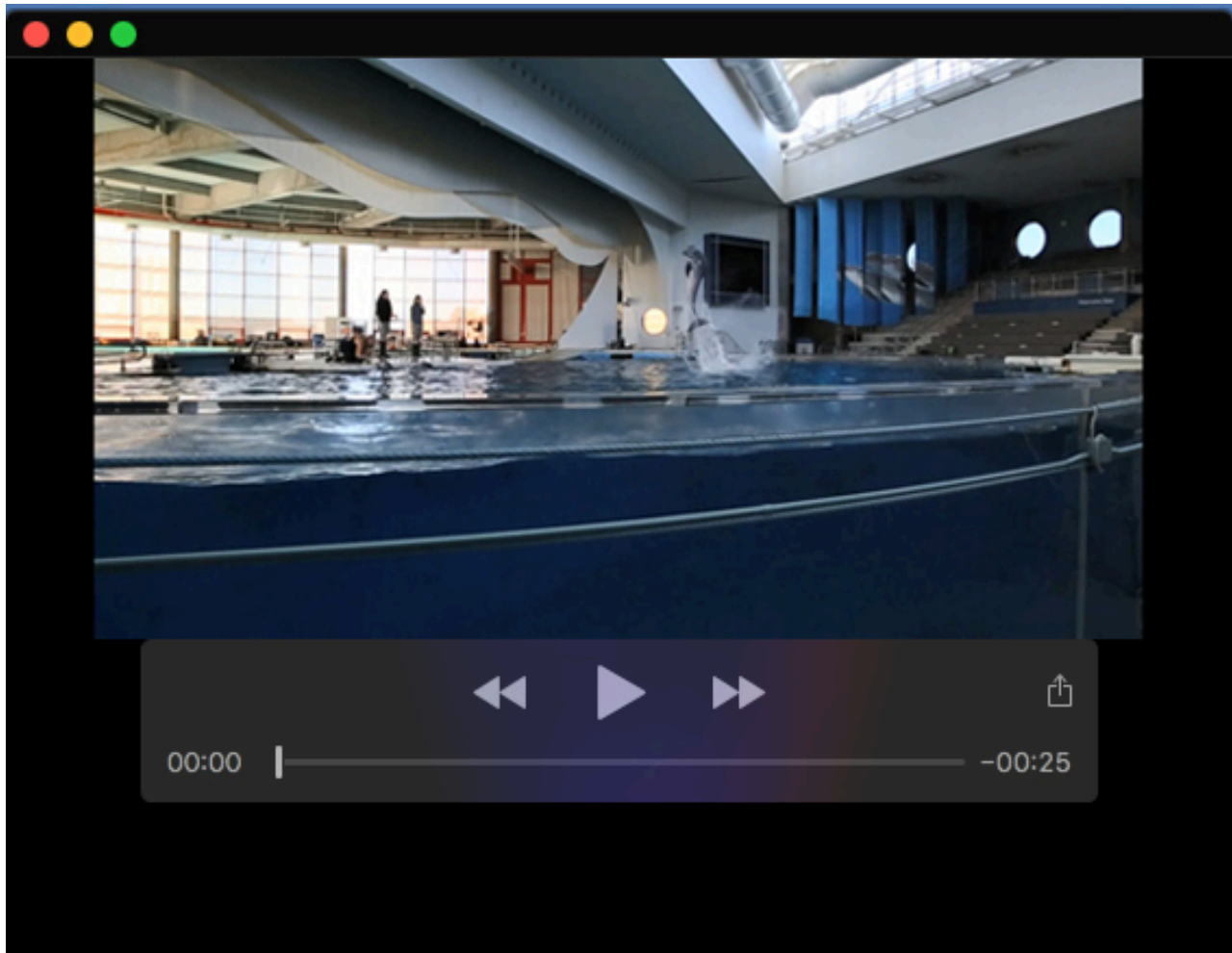
<https://www.youtube.com/watch?v=zZTQngw8MZE>

Whales breaching/ Huge jumps out of the water - Whale breaching

<https://www.youtube.com/watch?v=hq-j9UQF30g>



Movie 1. The video shows a Pacific white-sided dolphin (*Lagenorhynchus obliquidens*) during the underwater and aerial phases of a spinning leap. Underwater, the dolphin initiates a slow spin while swimming vertically toward the surface of the water. In the aerial phase, the dolphin leaps vertically about two body lengths above the water surface and increases its spin rate to 617.2 deg s^{-1} before falling back into the water.



Movie 2. The video shows the spinning leap of a bottlenose dolphin (*Tursiops truncatus*). The dolphin rises to a maximum of height of 1.6 body lengths above the water surface. The dolphin contorts its body so that it flips over and re-enters the water head-first. The aerial spin rate was about 490.9 deg s^{-1} .



Movie 3. Video recorded from a suction cup tag attached to the dorsum of a humpback whale during a spinning breach.